JOURNAL OF GUIDANCE, CONTROL, AND DYNAMICS
Vol. 23, No. 6, November–December 2000

Comparison of Two Navier–Stokes Methods with Benchmark Active Control Technology Experiments

Robert E. Bartels* and David M. Schuster†
NASA Langley Research Center, Hampton, Virginia 23681-2199

Two commonly used three-dimensional compressible Navier–Stokes codes are applied to select test cases from an experimental data set on a model known as the Benchmark Active Control Technology (BACT) wing. The BACT test provides data for the validation of aerodynamic, aeroelastic, and active aeroelastic control simulation codes. An overview will be presented of the two Navier–Stokes aeroelastic codes currently being used in an analysis of that data. A collection of results obtained by the two methods will be compared with the BACT experimental data for a wing with a statically deflected spoiler and statically and dynamically deflected aileron. Both methods employ structured computational fluid dynamics flow solvers and continuous surface modeling for the computation of complex moving control surface geometry. Motivation for this work is the development of an integrated computational aeroelasticity and active control simulation capability for the transonic flight regime and validation of that capability using the BACT wing data.

Nomenclature

C	=	wing chord (16 in.)
f	=	frequency of aileron oscillation, Hz
M	=	Mach number
Re	=	Reynolds number, based on wing chord
α	=	angle of attack, deg
$\delta_{\text{Ail.}}$	=	aileron mean deflection angle, deg
$\delta_{\text{Sp.}}$	=	spoiler deflection angle, deg
η	=	span-wise coordinate, $= y/y\text{tip}$
θ	=	aileron oscillation amplitude, deg

Introduction

THIS paper presents computations using the aeroelastic Navier–Stokes/Euler codes CFL3DAE[1,2] and ENS3DAE,[3] both of which are used extensively in steady and unsteady aeroelastic analysis. The first method, known as ENS3DAE, was developed in the late 1980s by Lockheed-Georgia under contract to the U.S. Air Force Research Laboratory. This program has been used to solve numerous aerodynamic and aeroelastic problems about a wide range of geometries including wings, wing/fuselage, propulsion, and integrated airframe/propulsion configurations. The second method, known as CFL3DAE, has been developed more recently at the NASA Langley Research Center. Although several aeroelastic versions of CFL3D have had limited application, the aerodynamic base version of the code has been used to analyze a very wide range of problems and has become a staple for computational aerodynamics research throughout the industry.

These two codes have recently been applied to select test cases from the Benchmark Active Control Technology (BACT)[4] test conducted in the NASA Langley Transonic Dynamics Tunnel (TDT). These tests were conducted for the purpose of providing data for the validation of aerodynamic, aeroelastic, and active aeroelastic control simulation codes. The extensive database from these experiments includes steady and unsteady pressures for a wide range of static and oscillatory spoiler and aileron deflections. It also includes aeroelastic data acquired by mounting the wing on a flexible mount known as a pitch-and-plunge apparatus. Unsteady pressure, flutter onset, and transient time history data of aeroelastic motion excited by control surface motion were acquired during these tests. Active flutter suppression control systems using spoiler and trailing-edge control surfaces were also tested.

The purpose of this paper is to highlight the BACT test data as a source for correlation with computational fluid dynamics (CFD) methods and present an overview of several Navier–Stokes codes currently being applied to an analysis of this data. Because there is continuing interest in the validation of fluid dynamic codes for viscous dominated problems, this database provides many test cases from which to draw. The relatively simple geometry and/or aerodynamic complexity of many of the test cases are ideally suited to analysis using the Navier–Stokes equations. These include transonic flows involving shock waves interacting with boundary layers, generation of vortices, and separated boundary layers. The complex flows induced by large spoiler and trailing-edge control surface deflections also warrant use of analysis methods of the class used here. In this paper steady and unsteady transonic flow computations for statically deflected and harmonically oscillating control surfaces will be presented, and computations from the two codes will be compared with experimental pressure data.

Although high-order CFD methods will be used, simplifications are made with respect to the modeling of turbulence and surface geometry. Surface geometry will be modeled using one continuous surface to represent both the wing and control surfaces. The two codes use finite difference (ENS3DAE) vs finite volume (CFL3DAE) discretizations, different dynamically deforming mesh schemes including surface and wake cut motion, and different approaches to the time accurate computation of the Navier–Stokes equations in the presence of a deforming mesh. The flow turbulence is also modeled using simplified equation sets. In the present computations the turbulence models to be used are the Spalart–Allmaras model[5] used in CFL3DAE and the Baldwin–Lomax model[6] used in ENS3DAE. These represent differing levels of simplification in the modeling of turbulence and thus should be expected to impact the results in at least some of the cases examined here.

This paper begins with a brief summary of the flow solvers to be used and of the geometry of the wing and control surfaces to be modeled. This is followed by a discussion of computational results and comparisons with experiment. Steady results for deflected trailing-edge control surface (aileron) and spoiler will be presented first, followed by unsteady results induced by the harmonic oscillation of the aileron surface.

Solution Approach

Computational aerodynamics development has progressed at a rapid pace for nearly three decades, and these methods have become an invaluable tool for aerodynamic analysis and design. However,

Received 10 August 1999; revision received 8 February 2000; accepted for publication 3 March 2000.

*Aerospace Engineer, Aeroelasticity Branch. Senior Member AIAA.
†Aerospace Engineer, Aeroelasticity Branch. Associate Fellow AIAA.

the majority of the development has focused on steady aerodynamic simulations, and the algorithms and codes have been optimized for these types of problems. Only recently have researchers begun to seriously apply higher-order computational methods to three-dimensional unsteady flows. For these problems temporal accuracy is as important to the analysis as is spatial accuracy. The damping properties of both the spatial and temporal components of the algorithm play a large role in the ability of a given method to accurately predict unsteady flows. This is especially true for self-excited unsteady flows such as periodic vorticity shedding caused by separation and shock boundary-layer interaction. Therefore, we will compare results from two computational aeroelasticity algorithms that take significantly different approaches to the solution of the aerodynamic equations of motion. It is not our purpose to assess the preceding questions much less to answer them, but rather to stimulate further research in this area by comparing results using different algorithms on a realistic unsteady aerodynamics problem for which experimental data is available.

ENS3DAE

ENS3DAE solves the full three-dimensional compressible Reynolds-averaged Navier–Stokes equations using an implicit approximate factorization algorithm. Central finite differences are used to spatially discretize the problem. A three-dimensional implementation of the Beam–Warming implicit scheme is employed for the temporal integration. Blended second- and fourth-order dissipation is added to the explicit right-hand side of the equations, and implicit second-order dissipation is added to improve the diagonal dominance of the matrix system. The method accepts either single- or multiple-block curvilinear grid topologies and can be run in a steady state or time-accurate mode by specifying local or global time stepping, respectively. Turbulence characteristics are predicted using the Baldwin–Lomax algebraic turbulence model or the Johnson–King model. For the present calculations the Baldwin–Lomax model is used with transition assumed to be at the leading edge of the wing. A multigrid option for steady flows has recently been added to the method, and the code has been explicitly written to take advantage of vectorization. Directives for parallel operation on shared memory processors are also included in the programming, and the method is regularly run on eight or more processors.

A linear generalized mode shape structural model is closely coupled with the aerodynamic method to analyze structurally flexible vehicles. Modal motion is also used for prescribed control surface motion. Figure 1 presents the manner in which the two codes move the wake cut in response to trailing-edge motion. As can be seen in this figure, ENS3DAE moves the wake cut by extending the line through the trailing edge horizontally to the downstream point. Because dynamic aeroelastic and oscillating control surface simulations require grid models that deform in time, a geometric conservation law (GCL)[7] has also been incorporated in the code.

CFL3DAE

CFL3DAE solves the thin-layer three-dimensional compressible Reynolds-averaged Navier–Stokes equations. The integral form of the equations is spatially discretized with volume integrals evaluated at cell centers and fluxes evaluated at cell faces. Typically, upwind differencing of the fluxes is used. Here, third-order upwind-biased Roe's flux difference splitting and a minmod flux limiter and second-order-accurate backward time differencing are used. An implicit approximate factorization algorithm is used to solve the equations. Physical time subiteration (t-TS) and local (Courant–Friedrichs–Lewy) based pseudotime subiteration (τ-TS) are available. Typically the τ-TS method is employed to accelerate convergence at each time step. CFL3D version 5.0, on which the current aeroelastic version of the code is based, includes many turbulence models. The turbulence model used in the present computations is the Spalart–Allmaras model, used here because of its performance in the presence of separated flow and because of past excellent performance in computations with large time step. The turbulence in this model evolves naturally from the leading edge.

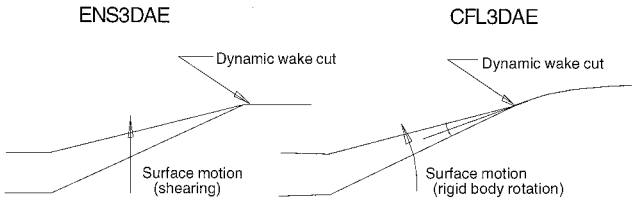

Fig. 1 Surface motion and dynamic wake cut modeling.

There have been several aeroelastic versions of the code developed. The present version incorporates a new deforming mesh scheme based on the spring analogy and incorporates the GCL into the Navier–Stokes equations.[2] Special attention has been paid to treatment of the grid at wall boundaries and in the wake. In particular, the orthogonality of the grid points within the boundary layer is maintained even at large surface deflection. Frequently, shearing or one- or two-dimensional modal motion is used to model control surface motion, each of which introduce distortion. The present CFL3DAE code models prescribed wing or control surface motion as true solid body motion, eliminating this potential source of solution error. The movement of the wake cut has also been addressed. Referring again to Fig. 1, CFL3DAE extends the wake cut from the trailing edge by bisecting the trailing-edge upper and lower surfaces. An exponential decay downstream returns the wake cut to a horizontal asymptote well before one chord length has passed. Although not used in the computations discussed in this paper, the code also has static and dynamic aeroelastic capability. For the simulation of unsteady responses, a closely coupled time-marching solution of the aeroelastic equations of motion is obtained using a predictor-corrector linear finite dimensional state-space formulation of the uncoupled modal equations.[8]

BACT Wing Geometry and Experimental Data

The NASA Langley BACT wing is used to perform all simulations presented in this paper. A schematic of its geometry can be found elsewhere.[9] The BACT model is a rectangular wing with a NACA 0012 airfoil section. The wing has a semispan of 32 in. (81.28 cm) plus tip of revolution and a chord of 16 in. (40.64 cm). It is fitted with an aileron (trailing-edge) control surface that extends from 45 to 75% span and has a chord of 25% of the wing chord. The wind-tunnel model also had upper and lower surface spoilers, which extend from 60 to 75% chord and over the same span as the aileron. The spoilers were not constructed to conform to the airfoil shape, but rather had flat external surfaces. This is in contrast to the surface shape used in the computational model, which did not account for the flat spoiler surface, using rather the theoretical airfoil shape. Experimental data for this wing include overall wing forces and moments as well as unsteady pressures. A row of pressure transducers were located on the upper and lower surfaces of the wing at 60% span, which coincides with the span-wise center of the aileron and spoilers. Pressures were measured from the wing leading edge to the trailing edge at this wing station. In addition, a second row of pressure transducers was located at 40% span. At this location upper and lower surface pressures were measured from 60% chord to the wing trailing edge. The model also included a transition strip at 10% chord.

Because the BACT wing has a blunt leading-edge, 12% thick airfoil section, a C-H grid topology is used to model this configuration. This grid consists of a total of 332,469 grid points distributed with 153 points in the wraparound or C direction, 53 points in the span-wise or H direction, and 41 points from the wing surface to the outer boundary. This grid was used in the computations performed by both codes. An isometric view of the BACT surface grid with the aileron deflected -5 deg is presented in Fig. 2. The grid lines are placed in the span-wise direction to accurately define the edges of the trailing-edge control surface. In addition, there is a grid line precisely at 40 and 60% span so that a direct comparison can be made with available experimental data. The stream-wise distribution and clustering of grid points is also tailored to model accurately the aileron hinge line. The aileron deflection for the static cases is obtained by preprocessing the airfoil sections used to define the wing surface. A rigid-body rotation of the trailing-edge portion of the airfoil sections at the inboard and outboard edges of the control surface is performed to define new airfoil contours at

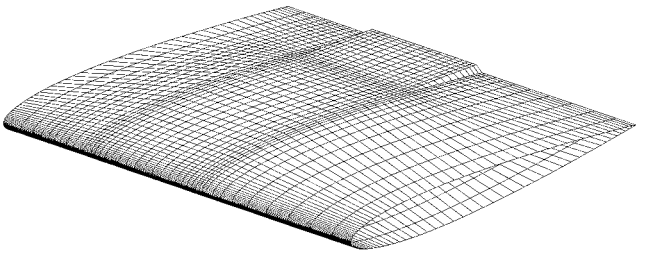

Fig. 2 Isometric view of BACT wing surface grid with aileron deflected ($\delta_{Ail.} = -5$ deg).

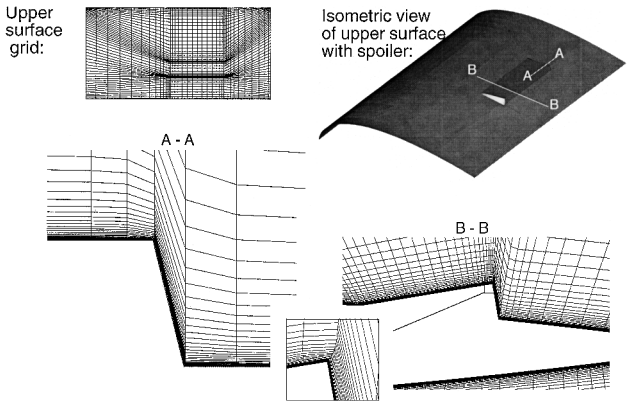

Fig. 3 Surface and flowfield grids for upper surface spoiler deflected ($\delta_{sp.} = -15$ deg).

these wing stations. The airfoils just inboard and just outboard of the aileron are left unchanged. The flowfield grid is then generated about this modified geometry using the same techniques as for the case where the aileron is not deflected. This method is simple and very efficient to implement. However, the result is a model that does not have gaps between the control-surface span-wise edges and the main wing. Although not a significant problem for analyses involving small control-surface deflections, for which these gaps will be small, the error caused by this model can become significant when large control-surface deflections are simulated.

The continuous surface approach is also used for the spoiler, modeled here as a ramp of finite span and backward-facing step. The upper surface spoiler and associated grid lines at a −15-deg deflection are shown in Fig. 3. Clearly, this approach does not model the effect of the cavity beneath the spoiler, nor the gap between the spoiler and flap leading edge. It does offer, however, a rapid, easily implemented approach to three-dimensional spoiler modeling in the context of a structured mesh scheme. Aside from these limitations in the surface modeling, the spoiler deflection is modeled with the correct rigid-body rotation about the hinge line, and clustering at each of the four spoiler edges is used to resolve the surface slope discontinuities. Over the backward step three surface grid points are spaced more or less evenly.

For cases where the aileron is oscillated, a mode shape describing the aileron deflection is input directly into the ENS3DAE program. The undeflected grid is used as the basis for the aerodynamic solution. The grid is deformed in time by superimposing the aileron deflection mode shape on the baseline grid and using ENS3DAE's built-in grid motion capability to deflect the grid. This method effectively shears the grid in the vicinity of the aileron, and control-surface gaps are not simulated. The mode shape is also defined as a deflection only in the vertical direction so that the chord of the control surface is stretched as the aileron is deflected. For small deflections this stretching is negligible. In the CFL3DAE program the harmonic aileron oscillation is accomplished by solid surface rotation. The near-surface fluid mesh also moves with the aileron, both in translation and rotation, exponentially decaying to a mesh obtained by a modified spring analogy. The advantage of this approach is that the original orientation of near-surface fluid grids is maintained through the entire range of motion. This approach results in a forward and aft motion of the surface grids and fluid mesh near the leading edge of the aileron, requiring that the mesh near the aileron leading edge be tested for grid line crossing at each time step. Surface grids are relocated as needed to maintain surface grid smoothness.

Results

BACT Wing Static Analyses

Static and dynamic rigid calculations were performed on the BACT wing with ENS3DAE and CFL3DAE providing viscous full and thin-layer Reynolds-averaged Navier–Stokes simulations. These calculations were compared with experimental data acquired in heavy gas in NASA Langley Research Center's TDT. The nominal flight conditions for these calculations are Mach 0.77 and a Reynolds number of 3.96 million based on the wing chord, which coincide with the test data acquired in the TDT.

Static calculations were performed with fixed aileron and spoiler deflections. Both ENS3DAE and CFL3DAE used grids having identical dimensions and nearly identical grid spacing for the static aileron cases. Figure 4 shows the pressure distribution for the ENS3DAE and CFL3DAE Navier–Stokes calculations at $M = 0.77$, $\alpha = 0.0$ deg, and $\delta_{Ail.} = 5.0$ deg. At these conditions the wing generates lift as a result of the aileron deflection. The comparison between ENS3DAE and CFL3DAE is good at these conditions, which represent a relatively small control-surface deflection. The overall character of the pressure distribution is the same for the two theoretical methods with relatively minor differences confined to the area between 20 and 60% chord. ENS3DAE also seems to round off the peak in the pressure distribution in the vicinity of the aileron hinge line. This is likely caused by the difference in the spatial formulation of the two codes. Upwind schemes, as used by CFL3DAE, have a demonstrated ability to capture sharper pressure discontinuities for shock waves than schemes based on central differences. It appears that this feature can further carry over to surface discontinuities like hinge lines. The theoretical and experimental pressures agree well

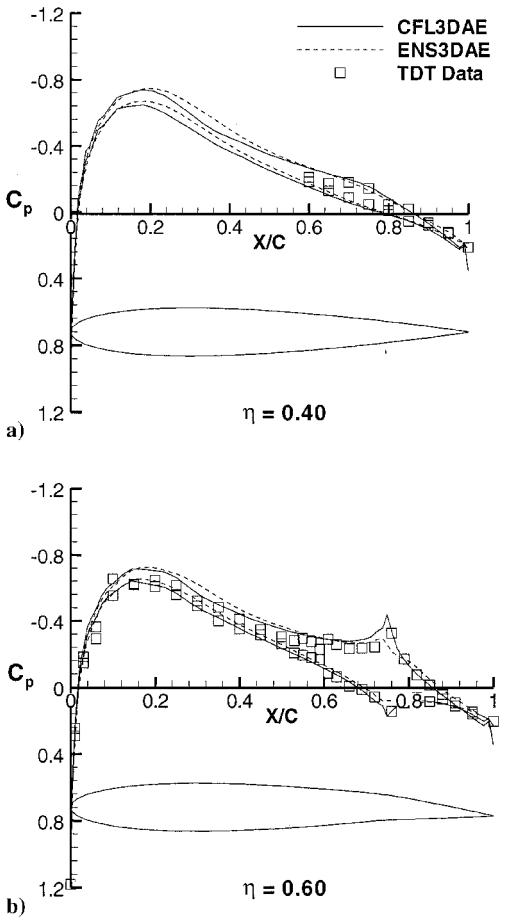

Fig. 4 Steady BACT pressures, $\delta_{Ail.} = 5.0$ deg, and $Re_c = 3.96 \times 10^6$.

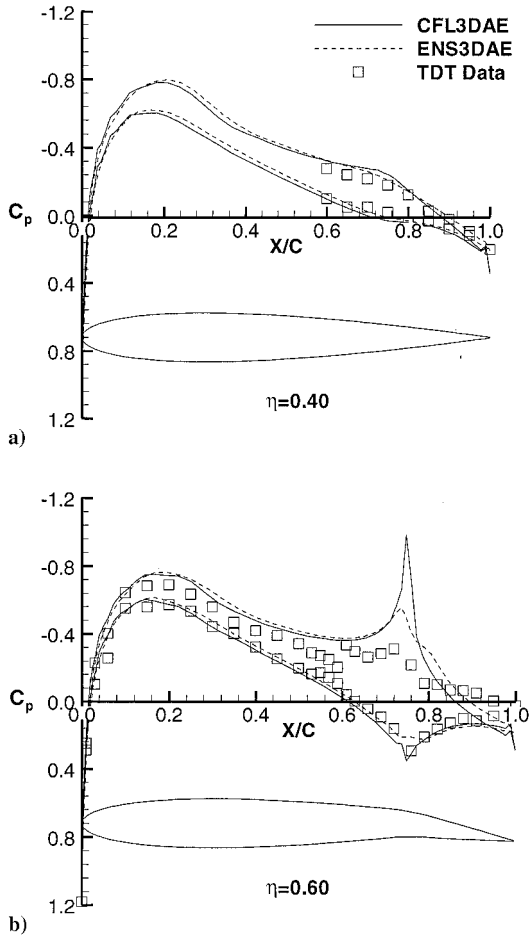

Fig. 5 Steady BACT pressures, $\delta_{\text{Ail.}} = 10.0$ deg, and $Re_c = 3.96 \times 10^6$.

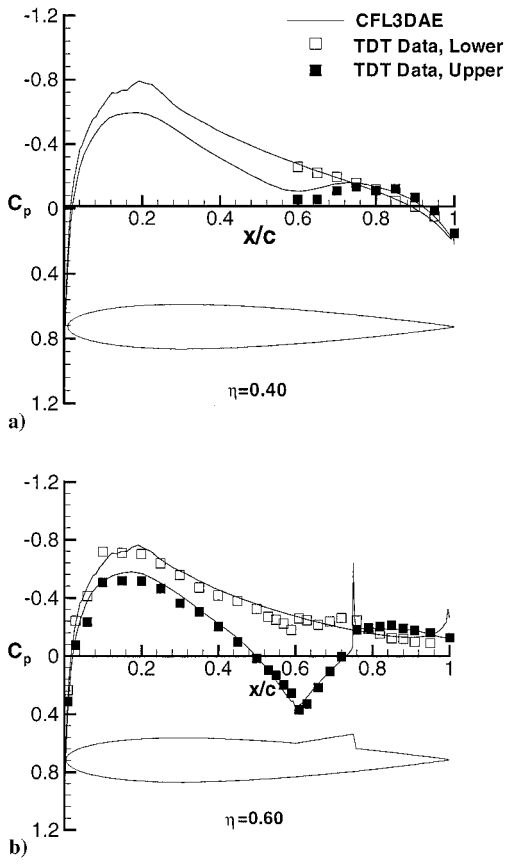

Fig. 6 Steady BACT pressures, $\delta_{\text{Sp.}} = -15.0$ deg, and $Re_c = 3.96 \times 10^6$.

on the aft portion of the wing and on the entire lower surface. However, the upper surface pressures, on the forward portion of the wing and just ahead of the aileron hinge line, do not agree well with the experimental data. The theory predicts a consistently lower pressure on these areas of the wing.

Figure 5 presents the pressure distribution for viscous solutions using the two codes at the same condition as in Fig. 4, but with $\delta_{\text{Ail.}} = 10.0$ deg. Comparing the two theoretical methods, this case produces similar behavior as the preceding case. The computed solutions agree well over the wing lower surface. However, the pressures are displaced from the experimental data over the entire upper surface of the wing. Both solutions are much different than experiment from just ahead of the spoiler hinge line to the trailing edge. The experimental data indicate a flow separation on the upper surface of the aileron beginning at 80% chord that is not predicted by either of the computations.

Figure 3 shows the surface and flowfield grid for a spoiler deflected at $\delta_{\text{Sp.}} = -15.0$ deg. To resolve the additional surface slope discontinuities of the spoiler geometry compared to those of the trailing-edge control-surface cases, a finer grid with dimensions $201 \times 73 \times 73$ was used. Additional grids in the directions spanwise, streamwise, and normal to the surface were added to capture somewhat better the reversed flow region and shear layer behind the spoiler trailing edge. Because of the added geometric complexity of the deflected spoiler, the Navier–Stokes equations in this computation included the thin-layer viscous terms in all three coordinate directions. A converged steady-state solution obtained with CFL3DAE at $M = 0.77$ and $\alpha = 0.0$ deg is represented in Fig. 6. The computed results show remarkably good agreement with the experiment, especially so when compared with the moderate comparison of the computations in Fig. 5 with the data. Although the results are not shown here, computations with a mesh having the same overall number of grids as was used in the aileron computations still showed very good agreement with the statically deflected spoiler data.

BACT Wing Unsteady Analysis

Unsteady simulations have been performed by harmonically oscillating the BACT aileron at a specified frequency and amplitude. The two codes used identically dimensioned grids for the dynamic case, however, with somewhat different clustering at the hinge line. The solution with CFL3DAE was made with more clustering of grids in the stream-wise direction at the hinge line, which will account for some of the differences in the dynamic results to follow. Furthermore, differences in the grid motion algorithms employed by the codes during the dynamic motion of the aileron caused the grids to differ as the dynamic solution progressed. Using a steady solution about the baseline condition without aileron deflection, the unsteady computations were performed by impulsively starting the aileron oscillation. The solution is allowed to progress until a total of at least three cycles of aileron oscillation are completed. For the simulations presented in this paper, the aileron is oscillated sinusoidally with an amplitude of 2 deg at a frequency of 5 Hz, which corresponds to a reduced frequency of 0.056 based on wing semichord.

The unsteady pressures at the 40 and 60% span station are analyzed by taking the fast Fourier transform of the pressures during the final cycle of aileron motion. The real and imaginary components are then scaled by the amplitude of the aileron deflection. In the next figures the real component of the unsteady pressure represents the pressure perturbation that is in-phase with the aileron motion, whereas the imaginary component represents the pressure perturbation whose phase lags the aileron motion by 90 deg.

The mean pressure during the aileron oscillation is also extracted from the theoretical and experimental data. Figure 7 compares the computed and experimental mean pressures for the oscillating aileron case. Here, the comparison between the two theories and the experimental data is excellent. The aileron motion for this case is symmetrical, and the wing is at 0 deg angle of attack, and so the mean pressure should be identical for the upper and lower surfaces for this symmetrical airfoil section. Both theories predict an identically symmetrical mean pressure distribution during the aileron oscillation.

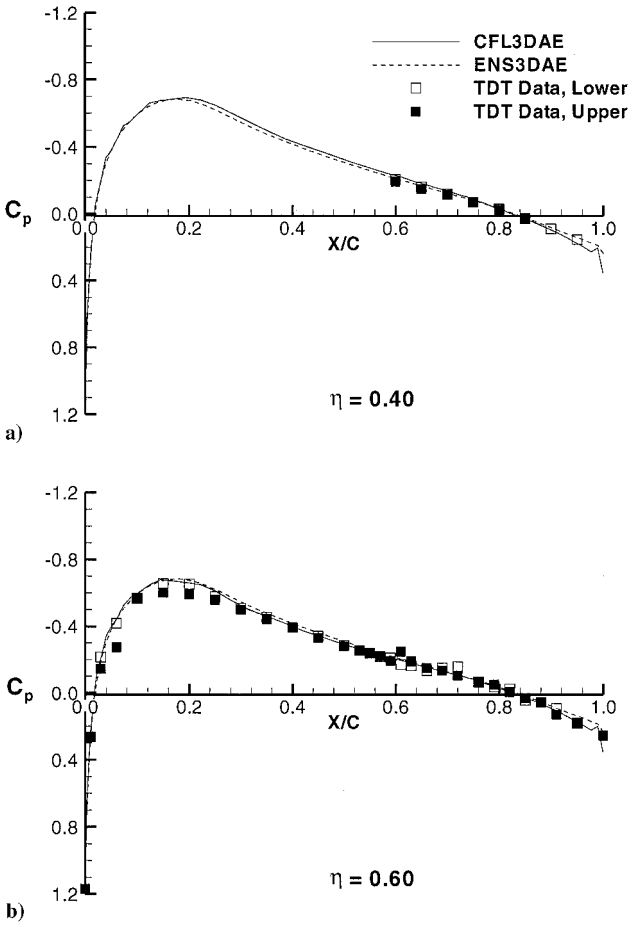

Fig. 7 Mean BACT pressures, $\theta_{\text{Ail.}} = 2.0$ deg, $f = 5$ Hz, and $Re_c = 3.96 \times 10^6$.

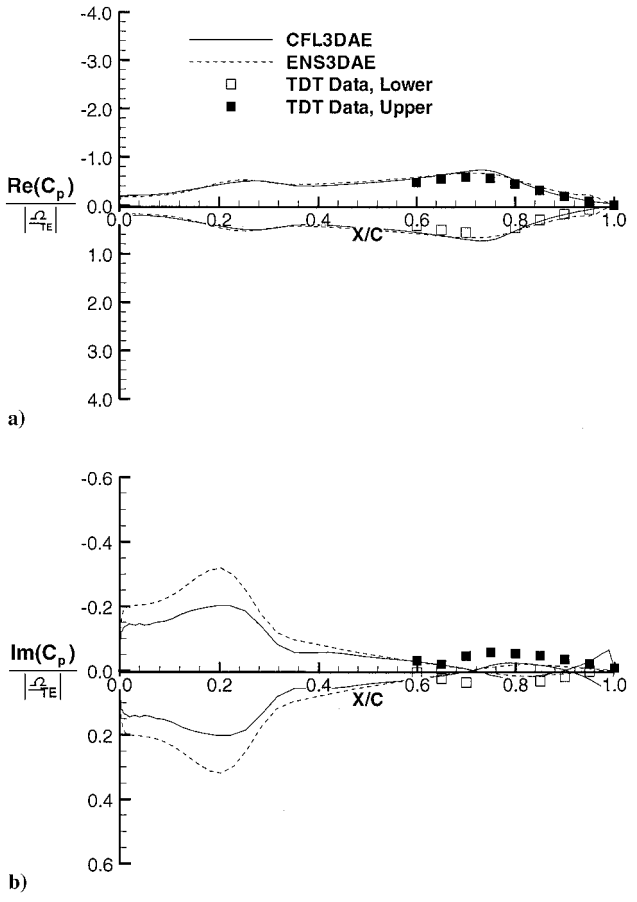

Fig. 8 Unsteady BACT pressures, $\theta_{\text{Ail.}} = 2.0$ deg, $f = 5$ Hz, $\eta = 0.40$, and $Re_c = 3.96 \times 10^6$.

Figure 8 compares the in-phase and out-of-phase perturbation pressures at the 40% span, whereas Fig. 9 presents this same comparison at 60% span. The vertical scale of the imaginary component is significantly expanded from that of the real component. Both of these figures show that at this low reduced frequency the pressure coefficient response to the aileron deflection is primarily in-phase with the aileron motion because the real components of the pressures are noticeably larger in amplitude than the imaginary components. The comparison of both the real and imaginary components of pressure with the experimental data are very good at the 40% span station. The in-phase components of the two computed solutions also compare favorably here. However, there is a notable difference in the computed out-of-phase components near the wing leading edge. This could become significant for flows where the in-phase and out-of-phase pressure components are of comparable magnitude.

The comparison is also good for the real pressure at 60% span from 60% chord aft. The jump in the experimental real component of the pressure in Fig. 9 is caused by the spoiler hinge line at 60% chord. This is not modeled in the present computations. The aileron extends from 75% chord aft, and the agreement between theory and experiment on this portion of the wing is excellent. In a notable similarity between the two computed solutions, it is significant that both show the crossover of the imaginary part at the same location, which is far aft of the point at which the experiment shows the crossover.

Finally, Table 1 compares the performance of the two codes for the unsteady case just discussed. This comparison represents the smallest number of time steps per cycle that could be taken by the two methods without adversely affecting solution accuracy. These data graphically reveal the difference in performance of the t-TS (ENS3DAE) and the τ-TS (CFL3DAE) methods of subiteration and the two approaches to flux differencing. CFL3DAE is capable of simulating this flow condition a full five times faster than ENS3DAE.

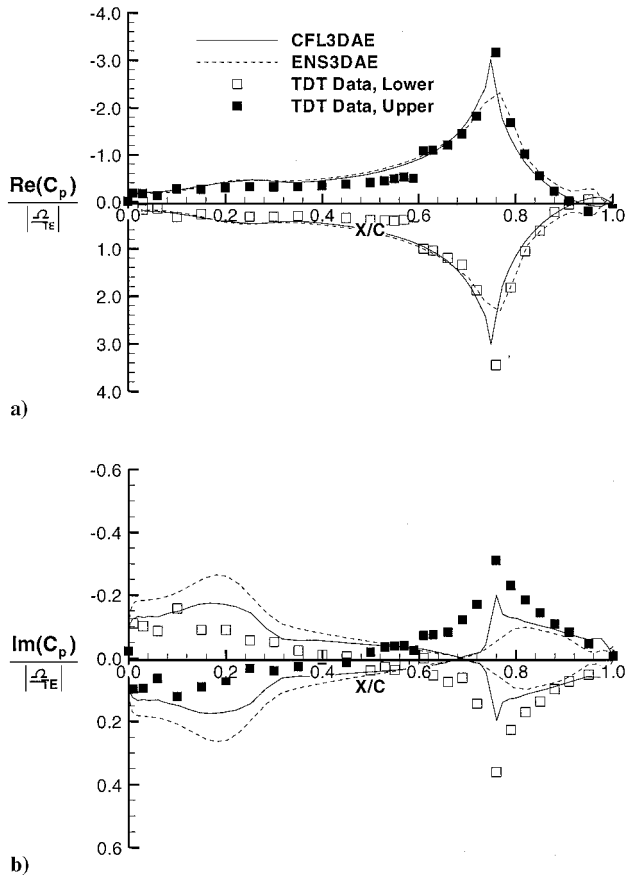

Fig. 9 Unsteady BACT pressures, $\theta_{\text{Ail.}} = 2.0$ deg, $f = 5$ Hz, $\eta = 0.60$, and $Re_c = 3.96 \times 10^6$.

Table 1 Code performance comparison

Method	Time steps per cycle	No. of subiterations	Method of subiteration	CRAY C-90 time/cycle, min.
ENS3DAE	3300	1	t-TS	175
CFL3DAE	128	5	τ-TS	35

Conclusions

Two computational aeroelasticity programs based on Navier–Stokes aerodynamics have been used to compute steady and unsteady flows about the BACT wing. The two methodologies, known as ENS3DAE and CFL3DAE, use significantly different approaches to the solution of the aerodynamic equations of motion as well as the implementation of their respective dynamic grid motion modules. Nevertheless, the two codes compare favorably when applied to the BACT wing with static and oscillating aileron deflections. At a static aileron angle of 5 deg, the two methods are in very good agreement with the experiment. At 10 deg aileron angle the two methods are significantly different from experiment. This is likely because neither computation predicts the separation on the upper surface of the aileron, at 10 deg deflection, exhibited in the experimental data. This separation very likely impacts the flow on the entire upper surface of the wing. It is speculated that the large-scale separation seen in the experimental data may be from a variety of geometry-related causes. It may be in part caused by influence of aileron side edge venting, spoiler surface discontinuities discussed earlier in this report, and possibly some pressure leakage between the aileron and spoiler hinge lines through the spoiler cavity. Modeling of this geometric complexity may be required to capture adequately the flow at large deflection. This conjecture is substantiated by the fact that the separated flow aft of the deflected spoiler is modeled well, indicating that the flow and turbulence model used in the deflected spoiler computation is adequate for that case and indeed for all of the cases considered here. The unsteady results have revealed several similarities and differences between the two codes and experiment. In general, the two codes agree well, with differences mainly between them and experiment. This may again be caused by the insufficiency of the geometric model used in the computations. Finally, a comparison of the performance of the two methods has been shown, revealing the difference in performance of the t-TS and the τ-TS methods of subiteration and the two approaches to flux differencing. For the present cases the τ-TS method has resulted in a significant increase in performance.

References

[1]Krist, S. L., Biedron, R. T., and Rumsey, C. L., "CFL3D User's Manual (Version 5,0)," NASA/TM-1998-208444, June 1998.

[2]Bartels, R. E., "An Elasticity Based Mesh Scheme Applied to the Computation of Unsteady Three Dimensional Spoiler and Aeroelastic Problems," AIAA Paper 99-3301, June 1999.

[3]Schuster, D. M., Vadyak, J., and Atta, E., "Flight Loads Prediction Methods for Fighter Aircraft," U.S. Air Force Wright Research and Development Center, WRDC-TR-89-3104, Wright–Patterson Air Force Base, OH, Nov. 1989.

[4]Scott, R. C., Hoadley, S. T., Wieseman, C. D., and Darham, M. H., "The Benchmark Active Controls Technology Model Aerodynamic Data," AIAA Paper 97-0829, 1997.

[5]Spalart, P., and Allmaras, S., "A One-Equation Turbulence Model for Aerodynamic Flows," AIAA Paper 92-0439, Jan. 1992.

[6]Baldwin, B., and Lomax, H., "Thin Layer Approximation and Algebraic Model for Separated Turbulent Flow," AIAA Paper 78-257, Jan. 1978.

[7]Thomas, P. D., and Lombard, C. K., "Geometric Conservation Law and its Application to Flow Computations on Moving Grids," *AIAA Journal*, Vol. 17, No. 10, 1979, pp. 1030–1037.

[8]Cunningham, H. J., Batina, J. T., and Bennett, R. M., "Modern Wing Flutter Analysis by Computational Fluid Dynamics Methods," *Journal of Aircraft*, Vol. 25, No. 10, 1988, pp. 962–968.

[9]Bartels, R. E., and Schuster, D. M., "Comparison of Two Navier–Stokes Aeroelastic Methods Using BACT Benchmark Experimental Data," *Proceedings of the 17th AIAA Applied Aerodynamics Conference*, AIAA, Reston, VA, 1999, pp. 433–443.